water

MDPI

Article

Ecological based flood energy dissipation by Single and Hybrid Defense System

Afzal Ahmed [1] and Abdul Razzaq Ghumman ,[1,2]

[1] Faculty of Civil and Environmental Engineering, University of Engineering & Technology Taxila, Rawalpindi 47080, Pakistan

[2] College of Engineering, Civil Engineering Department, Qassim University, Al-Mulida 51431, Saudi Arabia

* Correspondence: abdul.razzaq@uettaxila.edu.pk; abdul.razzaq@qec.edu.sa; Tel: +966-599-498859

Abstract: In this study a series of laboratory experiments were conducted to investigate the energy loss through the hybrid defense system (HDS) in the order of dyke (or embankment), moat/depression and emergent vegetation in steady subcritical flow conditions. A variety of experiments were performed for in-depth study of various options of energy dissipation. The results of HDS were compared with single defense system (SDS) comprising of only vegetation (OV). The dyke and moat were considered as unbreachable and the dimensions of dyke were kept constant while two different shapes (trapezoidal and rectangular) of moat were considered. The impacts of vegetation of variable thickness and density were investigated. Two combinations of HDS were investigated including the combination of dyke and vegetation (DV) and the combination of dyke, moat and vegetation (DMV). The effect of backwater rise on the vegetation upstream, hydraulic jump formation and arrival time of flood water on energy dissipation were measured and compared in each experiment/model. It was observed that on the upstream side of models, the backwater rise increased by increasing the Froude No. in both SDS and HDS. Whereas, the hydraulic jump was observed in HDS, which was classified and the energy dissipation due to hydraulic jump was also calculated. Under the current conditions, the maximum average energy dissipation was 32% in SDS and 46% in HDS. The trapezoidal moat performed better than rectangular moat as energy dissipater. The delay time was also greater with trapezoidal moat as compared to that in rectangular one. For each case of SDS and HDS, equations were developed by regression analysis to investigate the energy dissipation phenomena. The maximum delay time was 140s in case of HDS. Hence, the hybrid defense system offered maximum resistance to flow of water, thus causing a significant energy loss.

Keywords: Floods, defense system, vegetation, dyke, backwater rise, hydraulic jump, energy reduction

1. Introduction:

Heavy floods carry serious socio-economic threats. Annually, floods claim almost 20,000 lives and adversely affect at least 20 million people throughout the world[1]. The recent studies indicated that losses from flood hazards are expected to increase in near future, some attributing this to climate change [2]. In various European countries when flood arrived, the surrounding rivers also flood at the same time creating heavy damage to properties and human lives [3]. In 2011, the great East Tsunami in Japan arrived with a return period of 1000 years [4] destroyed embankments, coastal forests, tsunami gates and especially thousands of human lives [5,6,7]. Similarly, the other south Asian countries also affected by heavy floods in the recent past. Pakistan faces extreme flood events almost every year in the recent past and the statistical analysis shows that, a financial loss of US$ 38.165 billion, more than 12,000 human being causalities and 616,598 km^2 land area was affected as a result of 23 major flood events from 1947-2015 [8]. The extreme flood events in India resulted with death of large people in in Uttarakhand 2013, in Chennai 2015 and the most devastating in Kerala 2018 [9,10]. Almost 38 districts were affected by a continuous spell of heavy rainfall in Bangladesh in 2017 [11]. Same as other countries, Indonesia is also vulnerable to flood damages. [12,13].

In the last decade many researchers proposed "hard solutions" and they investigated the energy mitigation and flow phenomena over erodible and non-erodible embankments using physical model, numerical model and prototype analysis [14–17]. These methods can prove costly for developing countries because of huge capital investment requirement [18]. Currently, ecological based natural methods are widely considered in many developed and under developed countries [19–[23]. Ecosystem degradation is a major cause of increasing water resources management challenges [24–[28]. In the floodplain of rivers, vegetation tends to increase the hydraulic resistance by dragging and turbulence [26]. Consequently, increasing tree cover is promoted as an effective means to enhance the storage capacity of catchment areas to increase the lag time, reduce discharge and flood risk [27].

In addition to the above-mentioned solutions, the hybrid or compound defense system were also studied by different researchers. Various studies consist of the energy dissipation through a compound defense system of vegetation and a backward-facing step [28], the combined effects of sea embankment and coastal forest by using the field survey data [4,29], a moat with/without a forest [30] and a double embankment system [31]. Furthermore, Zaha (2019) conducted a series of experiments to investigate a hybrid defense system consisting of a forest, a moat (depression at floodplain) and an embankment under unsteady flow conditions, considering the dyke as unbreachable [32]. In the recent catastrophic floods in various regions, soon after the breaching of embankments , the flood water expand into the entire floodplains within a short duration [33]. However, the barriers in the path of water causes delay in arrival of water at any point [32].

However, the energy dissipation phenomena of hybrid defense system and the effect of various shapes of the components of HDS still needs further investigation [4][32]. The flow structure due to hybrid defense system becomes more complex because of the formation of hydraulic jump. The jump characteristics and its location should be identified to improve the efficiency of the hybrid defense system against the destructive forces [4]. In present paper, the hydraulic jumps developed in SDS and HDS were classified depending upon the location of hydraulic jump and the Froude number.The energy dissipation due to the formation of hydraulic jumps was also calculated. In HDS the effect of the density of vegetation and the shape of moat on total energy dissipation was analyzed and equations were developed by regression analysis to calculate energy dissipation which has hardly been reported previously. The field survey of different reaches of Indus basin reveals that the cross boundaries (embankments) are unprotected due to lack of proper maintenance and the density of coastal forests are very low (Figure1a, 1b and 1c). In order to improve their performance, there is a dire need to repair existing damaged embankments and construct a new ecological based system of flood protection [34].

Therefore, the objective of this study was to clarify the energy dissipation phenomena in case of single defense system and hybrid defense system. The energy dissipation effects of each system were compared by keeping special attention to the backwater rise on the upstream side of models, formation of hydraulic jump and the arrival time of flood water. This study aimed to provide findings that will strengthen the hybrid defense system against the flood energy. The range of Froude numbers were selected on the basis of previous data of different locations on the Indus basin. The proposed defense system will be effective for protection of various floodplains. The flood water can also be stored in moat to act as a flood water harvesting structure. Imagery of proposed HDS at River Indus near Taunsa Barrage, Pakistan is shown in Figure 1d which can be used world-wide.

2. Materials and methods

2.1. Experimental apparatus and procedures

2.1.1. Flume characteristics

A glass-sided open channel flume of 10m length, 0.31m width and 0.5 m height with a constant bed slope of 1/500 was used for the laboratory experiments with different conditions as shown in Table 1. The field data of past 59 years of Jinnah barrage (on the upstream side) and Taunsa barrage (on the downstream side) located on the Indus basin provided by the Punjab Irrigation Department, Punjab, Pakistan was used to select the experimental range of Initial Froude number ($Fr_o = V/(gh)^{0.5}$, where V = depth-averaged velocity (m/s), g = gravitational acceleration (m/s^2), and h = water depth (m)). The initial Froude number (Fr_o) was defined with the velocity and water depth without any model placed in the channel. The calculated range of Froude Number at barrage was 0.17-0.59 and at Taunsa barrage was 0.10-0.59. The flow was subcritical (Fr_o <1) in all the cases. Froude similarity was used to set the model scale of the physical experiment. For creating subcritical conditions, the water depths (without any model) (h_o) selected in the experiments were 4.5, 5.3, 6.8, 7.3, 7.7, 8.2 and 8.5 cm, setting the initial Froude number (Fro) approximately equal to 0.40, 0.44, 0.50, 0.57, 0.60, 0.63 and 0.65. The scale for all the cases of the current experimental study was 1/100.

Table 1. Experimental Conditions of hybrid defense system

Case ID	Initial Froude No. (Fro)	Dyke	Moat	Vegetation Density (*B/d*)	*D* (*cm*)	W_v (*cm*)	*Vegetation thickness "dn" (No.cm)	Vegetation type

OVS	0.40, 0.44, 0.50,0.58,0.61, 0.63, 0.65	No dyke	No moat	2.13	1.88	18.36	181.67	Sparse
OVI	0.40, 0.44, 0.50,0.58,0.61, 0.63, 0.65	No dyke	No moat	1.09	1.254	8.17	198.31	Intermediate
DVS	0.40, 0.44, 0.50,0.58,0.61, 0.63, 0.65	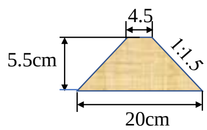	No moat	2.13	1.88	18.36	181.67	Sparse
DVI	0.40, 0.44, 0.50,0.58,0.61, 0.63, 0.65	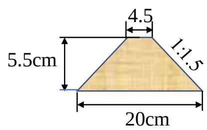	No moat	1.09	1.254	8.17	198.31	Intermediate
DTMVS	0.40, 0.44, 0.50,0.58,0.61, 0.63, 0.65	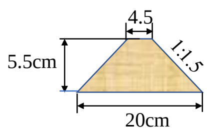	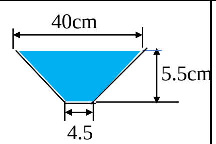	2.13	1.88	18.36	181.67	Sparse
DTMVI	0.40, 0.44, 0.50,0.58,0.61, 0.63, 0.65	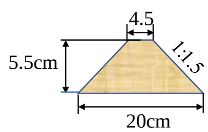	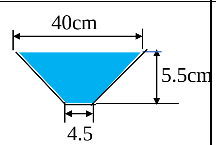	1.09	1.254	8.17	198.31	Intermediate
DRMVI	0.40, 0.44, 0.50,0.58,0.61, 0.63, 0.65	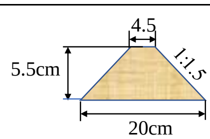	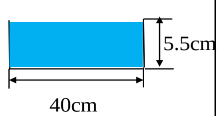	1.09	1.254	8.17	198.31	intermediate

** The initial value of value of "dn" was taken as 180No.cm. After inserting metal rods on wooden bed to make vegetation patch, the value of "dn" again calculated which was 181.67No.cm for sparse vegetation and 198.31No.cm for intermediate vegetation*

(a)

(b)

(c)

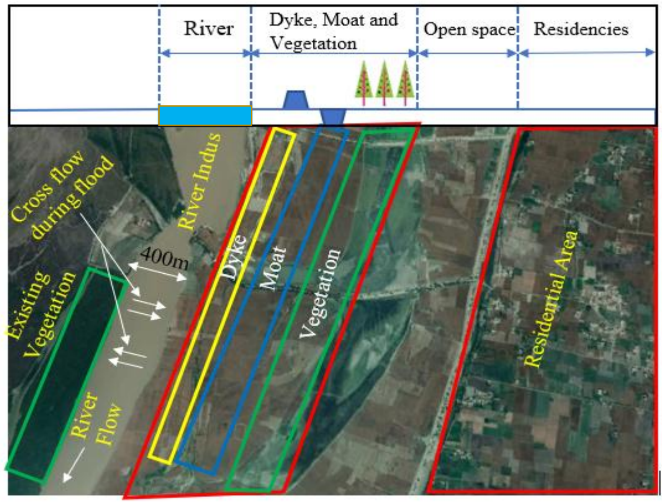

(d)

Figure 1. Pictorial views of floodplain of Indus River near Taunsa Barrage (a) Unprotected and scoured embankment (b) Stone embankment protection (c) Existing dyke and level gauge (d) Imagery of proposed HDS at River Indus near Taunsa Barrage

2.1.2. Experimental conditions

The tree species selected for the vegetation model was the Eucalyptus species; its tree crown was high relative to the maximum flood level in the past and the trees can be considered as circular cylinders [29]. The average tree height of that tree in the ecological zones of Punjab, Pakistan is in the range of 7.6-14.6 m and the average trunk diameter is in the range of 0.11-0.33 m [35]. To ensure the geometric similarity metal rods and steel cylinders of different diameters were used by various researchers [36],[37]. In this experimental work, keeping in view the above-mentioned limits of average tree diameter, metal rods of 0.003 m diameter at a scale of 1:100 were used because the wooden cylinders of such a small diameter was expected to break or bent during the experimentation. In SDS only vegetation (OV) models with variable densities i.e; sparse vegetation (OVS) having B/d=2.13 and intermediate vegetation (OVI) having B/d=1.09 were separately placed in the flume to check the individual capability of these models to dissipate energy, where B/d = vegetation density, B = spacing of each cylinder in cross-stream direction and d = diameter of cylindrical vegetation. The distance (D) between vegetation and width of vegetation patch (W_v) (Figure. 2c) were selected by considering the thickness of vegetation d_n =180 No.cm, where $d_n = \frac{2}{D^2\sqrt{3}} W_v d \times 10^2$ which represents the cumulative diameter of trees at breast height and defined as it *i*s the product of tree diameter and the number of trees in a rectangle with a frontage of unit length along the shoreline and depth equal to the width of the forest (W_v) [38].

In the current study dn = 180 was selected for both intermediate and sparse vegetation cases. The water level was measured by using a point gauge at the interval of 2–3 cm. Without placing any model in a flume, the discharge was measured using a flow meter against each selected initial water depth (h_o), and the discharge values against each initial water depth were noted. The depth-averaged velocity was computed using the measured water depth and discharge relationship. The dyke and the moat were modelled at a scale of 1/100. The recommended height of embankment (dyke) on Indus river in Pakistan is in the range of about 4–7m high with addition to 1.2-1.8m free board [39]. In the current study the height of embankment (including the free board) was selected 5.5m. Therefore, by using the scale of 1/100, the height of the model of embankment was kept 5.5cm. The dimensions of dyke and moat are already mentioned in Table 1.

The flood energy dissipation defense system was tested in two cases namely; single defense system (SDS) and the hybrid defense system (HDS) as elaborated in the schematic Figure 3. In HDS, a combination of a dyke and vegetation (DV) and combination of a dyke, moat and vegetation (DVM) models were tested separately. To clarify the effects of the hybrid defense systems on flood energy mitigation, the orders of the dyke, moat and vegetation was kept constant in all cases (Figure 2a). For expressing the respective cases in this study, the name of each model, D, M, V were used to represent 'Dyke', 'Moat', 'Vegetation' and OV= only vegetation, OVS = only sparse vegetation, OVI= only intermediate vegetation, DV = dyke and vegetation, DVS = dyke and sparse vegetation, DVI = dyke and intermediate vegetation, DMV= dyke, moat and vegetation, DTMVS = dyke, trapezoidal moat and sparse vegetation, DTMVI = dyke, trapezoidal moat and intermediate vegetation and DRMVI = dyke, rectangular moat and intermediate vegetation respectively. The models covering the full width of the channel were mounted in the water flume bed about 4 m from the upstream inlet.

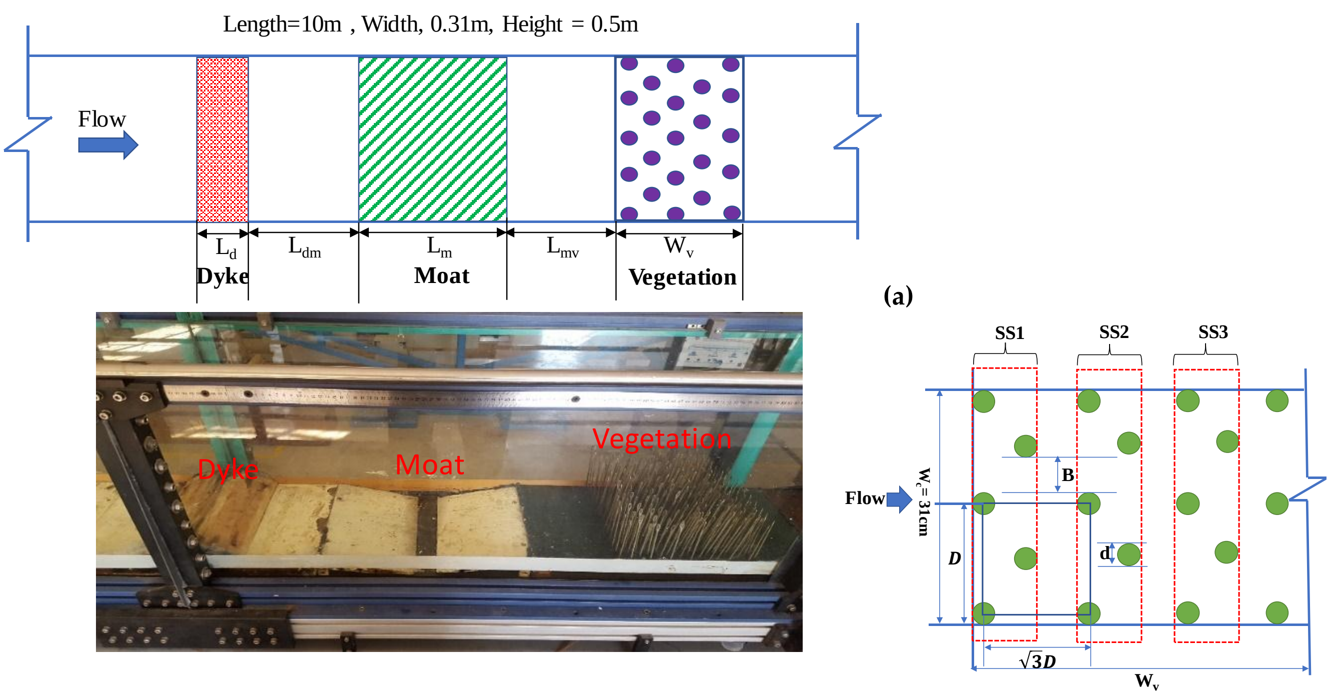

(b) (c)

Figure 2. Experimental Setup (a) Schematic of channel with models, (b) Experimental setup of hybrid defense system in laboratory, (c) Vegetation arrangement details of staggered strips (SS)

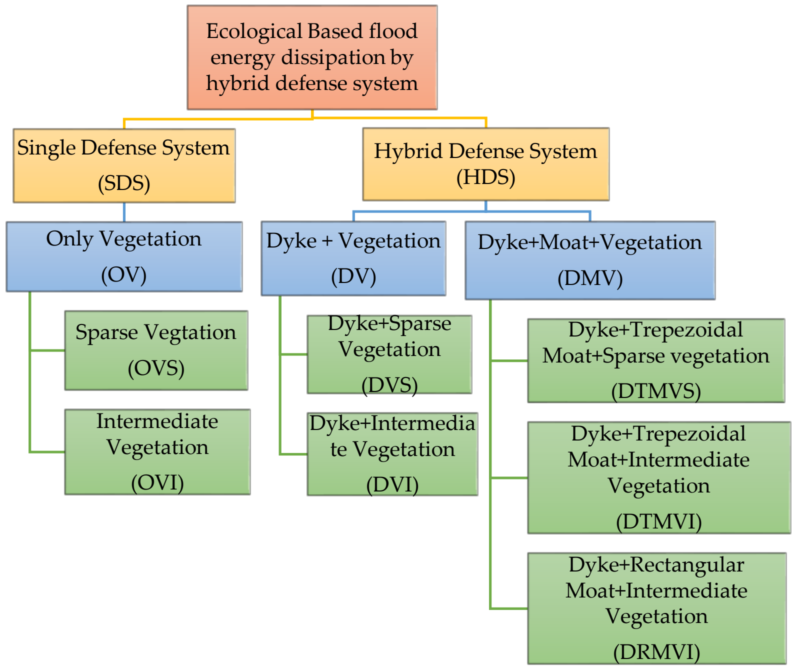

Figure 3. Schematic diagram of Experimental Model

2.2. Non-dimensional pi groups

The Scaling of experimental results to prototype conditions is challenging [40]. Figure 4 shows a flow structure scheme and important parameters of the proposed HDS. Flow conditions, type of structure, vegetation arrangement and their combination are the main parameters that decide the amount of energy lost, the following dimensionless groups were developed by using well known Buckingham's pi theorem

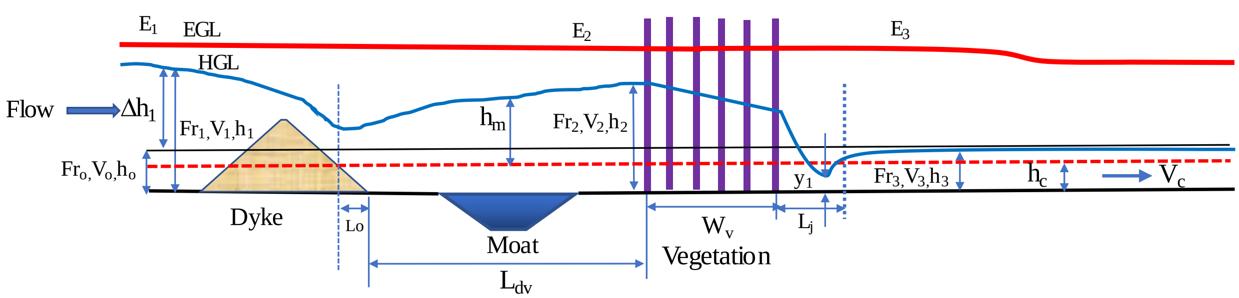

Figure 4. Experimental model of Hybrid Defense System (HDS)

$$f\left[\frac{\Delta h_1}{h_o}, \frac{\Delta h_2}{h_o}, \frac{\Delta h_3}{h_o}, \frac{\Delta h_1}{L_o}, \frac{\Delta h_2}{h_m}, \frac{v_o}{\sqrt{gh_o}}, \frac{v_1}{\sqrt{gh_1}}, \frac{v_2}{\sqrt{gh_2}}, \frac{v_3}{\sqrt{gh_3}}, \frac{\rho_w h_o v_o}{\mu}, d_n', \frac{B}{d}, \frac{h_3}{y_1}, \frac{L_j}{y_1}, \frac{v_2}{v_1}, \frac{v_3}{v_2}, \frac{\Delta E_1}{E_1}, \frac{\Delta E_2}{E_2}\right]=0$$

where Δh_1 = backwater rise at the upstream of dyke, h_o = initial water depth without any model, V_o = velocity at h_o, Fr_o = Froude number at h_o, Fr_1 = Froude number on the upstream side of dyke against water depth h_1 and velocity V_1, Fr_2 = Froude number in front of vegetation patch against water depth h_2 and velocity V_2, Fr_3 = Froude number on the downstream side of the vegetation patch against water depth h_3

and velocity V_3, g = gravitational acceleration, ρ_w = density of water, μ = viscosity of water, $d_n' = dn/D$ is non- dimensional vegetation width , y_1 = minimum water depth during the jump on the downstream of vegetation, L_j = length of hydraulic jump on the downstream of vegetation, *HGL* = hydraulic grade line, *EGL* = energy grade line, E_1, E_2, E_3 = specific energies at respective points, ΔE_1 = total energy loss $(E_1\text{-}E_3)$, ΔE_2 = total energy loss $(E_2\text{-}E_3)$, *dn*, *d* and *B* are already define in section 2.1.2. After the arrival of flood, inundation occurs when river water overtopping on embankment or breaching of embankment occurs. During overtopping or breaching phenomena, the river flow (top to bottom) can be considered as a perpendicular flow to the fenders [41]. To minimize the sidewall effects on the flow structure the ratio between the flume width and the cylinder diameter should be greater than 5 [4],[42]. In this study, this ratio was kept greater than 5 to minimize the sidewall effect. The backwater rise i.e; $\Delta h_1/h_o$, $\Delta h_2/h_o$ and total energy loss $(\Delta E_1/ E_1)$ and $(\Delta E_2/ E_2)$ are a function of the initial Froude number Fr_o, vegetation density (B/d) and d_n'. Froude number is commonly used in free surface flows, so the Reynolds number was not considered here.

$$\frac{\Delta h_1}{h_o},\frac{\Delta h_3}{h_o},\frac{\Delta E_1}{E_1},\frac{\Delta E_2}{E_2}=f\left[\frac{v_o}{\sqrt{gh_o}},\frac{B}{d},d_n'\right]$$

2.4 Description of Energy dissipation

The effectiveness of the hybrid defense structure was assessed by calculating the energy reduction (ΔE) in two ways. One was the reduction due to the formation of hydraulic jump within the hybrid defense system, and the other was the total energy dissipation by HDS. Energy reduction due to hydraulic jump in section 2 and section 3 are represented as $(\Delta E_{j2}/y_1)$ and $(\Delta E_{j3}/y_1)$, where, $\Delta E_{j2}, \Delta E_{j3} = \frac{(y_2-y_1)^3}{4y_1y_2}$ [43] and y_1 is the minimum depth at the toe of the hydraulic jump y_2 is the average water depth after the hydraulic jump.

The specific energy is defined as the energy per unit volume of water at any section of a channel with respect to the channel bed [44]. Therefore,

$$E=y+\alpha\frac{v^2}{2g} \quad (1)$$

where E = specific energy, y = water depth, v = velocity, and α = coefficient to account for variations in velocity, in this study a rectangular channel with a uniform cross-section and a constant discharge was taken, so the value of α is assumed to be unity as considered in the previous research [45]. The depth-averaged velocity against the known discharge (Q) was calculated using the known relationship for steady flow i.e; $V= Q/A$. The relative percentage energy loss was calculated by using equation 2 for DV and DMV models and equation 3 for OV models.

$$\Delta E_1=\frac{E_1\text{-}E_3}{E_1}x100 \quad (2)$$

$$\Delta E_2=\frac{E_2\text{-}E_3}{E_2}x100 \quad (3)$$

Where, ΔE_1 is the relative energy loss, E_1 = energy on the upstream side of dyke in DV and DMV models, E_2 = energy on the upstream side of vegetation and E_3 = energy on the downstream side of vegetation.

2.5 Delay time analysis

In this study the delay time is considered as the time required for water to reach from the inlet of 10m flume to the crest of the crump weir (Figure. 7d) installed at 800cm from the inlet having length = 70cm, width =31cm (throughout the channel width), height = 15cm, 1:5 slope on the upstream and 1:2 on the downstream side of crump weir. The time (T_{WM}) required to reach water from inlet to the crest level of the crump weir was noted without placing any model in the channel and compared with time required in SDS and HDS models.

3. Results

3.1. Back water rise

The vegetation always provides a barrier in front of water flow which creates backwater on the upstream side of the vegetation [30,[32] [30,][40]. In case of OVS and OVI the initial water depth (h_o) was raised upstream of the vegetation model, and the water surface slope was increased inside the vegetation due to the resistance offered by the vegetation. It was resulted that by increasing the density of vegetation from sparse to intermediate, the back water-rise increases to 26% and relative backwater rise increased to 30%, the surface slope inside the vegetation was also increaseds. The backwater rise and relative backwater rise varied linearly with increasing Froude number as shown in Figure 5a, 5b. However, the relative backwater rise was only slightly increased for different Froude conditions as the range of the values on y-axis was lower as shown in (Figure 5b, the similar trend was observed in the literature [40]). This shows that the initial flow depth had very little effect on the relative backwater rise for a given Froude number. In these Figures Δh and h_o are the water depths on the upstream side of vegetation and initial water depth without any model placed in the channel respectively.

Similarly, the dyke and vegetation (DV) together will offer more resistance to flow and back water rise also shared by both models. In this study it was observed that after placing dyke on the upstream side of vegetation, the maximum back water-rise increased was 15% and maximum relative backwater rise increased 19%. \The backwater rise in DVI was 8.50% greater than DVS. The DMV model offers more resistance to flow of water which resulted in higher backwater rise as compared to the previous models because of the moat. By placing the moat in between dyke and vegetation, backwater rise and relative backwater rise wasere increased to 21% and 22% respectively. By increasing the initial Froude no. backwater rise and relative backwater rise increases linearly in DTMVI, DRMVI and DTMVS models (Figure 5a, 5b). By increasing the density of vegetation, the model DTMVI shows 23% 24% more backwater rise and relative backwater rise respectively as compared to DTMVS. In DTMVI thisese values were 12% higher than DRMVI model. For the lower values of Froude number i.e; Fr_o = 0.40 and 0.44, the backwater rise was a little higher in SDS than HDS and for the remaining values HDS was higher, this was because in HDS for lower values of Fr_o the depth of water overtopping the dyke was low so the depth achieved in front of vegetation was also low. However, for higher values of Fr_o the overtopping depth was high and due to which higher depth was achieved on the upstream side of vegetation.

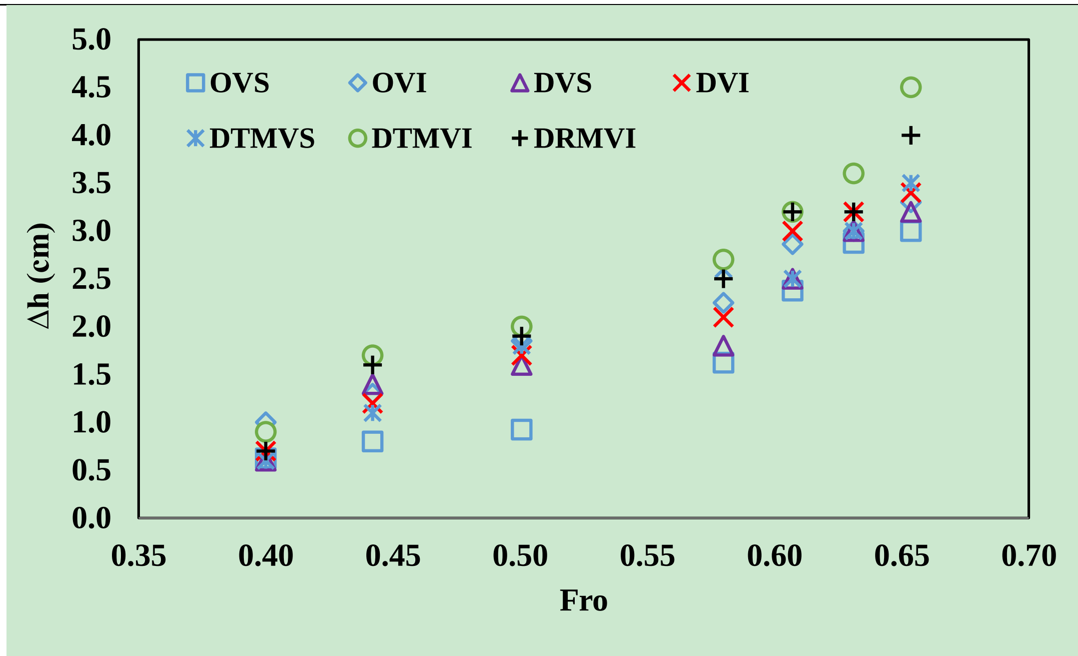

(a)

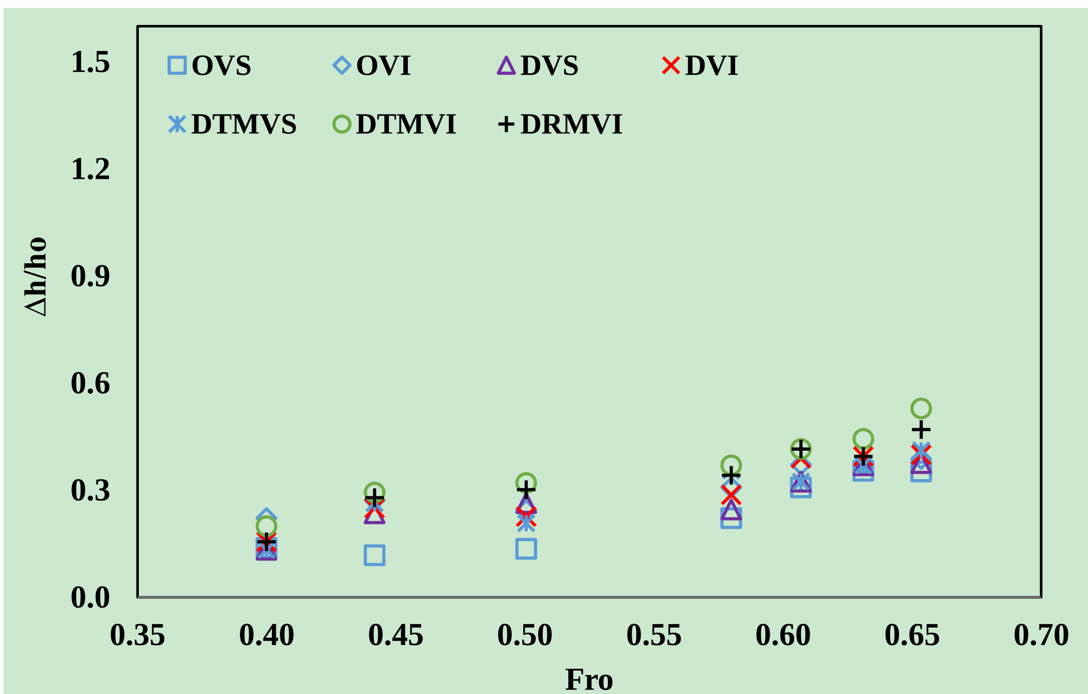

(b)

Fig. 5: (a) Back water rise (Δh) of SDS and HDS, (b) Realtive backwater rise (Δh/ho) of SDS and HDS

3.2 Hydraulic jump and water surface profile classification

A hydraulic jump is formed when supercritical flow transformed to subcritical flow [38]. Previously, various researchers studied and classified the formation of hydraulic jump due to only vegetation [40] and due to the combine effect of dyke and vegetation [4]. In the hybrid defense system the formation of hydraulic jump varied with changing flow and vegetation conditions and jump type varied by initial Froude number Fr_o [4]. It is important to control the position of a hydraulic jump to reduce the flow energy and to stabilize the hydraulic structure [46]. Thus, the jump type and associated water surface profiles and their classification in the hydraulic structures ~~is~~are essential for understanding the mitigation effect of a defense system. The types of jumps formed in this experimental investigation are classified in six different types depending upon the location of the jump as shown in Figure 6, whereas Figure 7 represents experimental photographs captured during the experimentation. The hydraulic jump was observed in between dyke and vegetation model (Section 2 in Figure 6) and/or on the downstream side of vegetation (Section 3 in Figure 6).

3.2. Hydraulic jump classification in SDS

In SDS the hydraulic jump formed is classified as Type I shown in Figure 6(a). In case of sparse vegetation (OVS) for initial values of Froude numbers i.e; Fr_o = 0.40, 0.44, 0.50, 0.57 and 0.60 only backwater rise and small undulations on the downstream side of vegetation with no hydraulic jump was observed while the flow has higher slope inside the vegetation patch. However, for remaining Froude numbers i.e; Fr_o = 0.63 and 0.65 an undular jump ($1<Fr<1.7$ [47]) was developed on the downstream side of vegetation patch (Type I) as shown in Figure 6a. Similarly, in case of intermediate vegetation (OVI) there was no jump formed against the lower values of Fr_o = 0.40, 0.44, 0.50 and 0.57, however, for Fr_o = 0.60, 0.63 and 0.65 undular jump was formed on the downstream side of vegetation patch (Type I). The classification of hydraulic jump of SDS is also elaborated in Table 2. The higher~~more~~ backwater rise, larger undulations and a larger undular jump was observed in OVI as compared to OVS. The relative length of hydraulic jump L_j/y_1 was maximum against Fr_o = 0.65 in OVI case. In Figure 6a h_1 and h_2 are the average depths of water on the upstream and downstream side of vegetation after the jump, y_1 = minimum depth of water in hydraulic jump, L_j = length of hydraulic jump, hc = critical depth, V_1, V_2 are the average velocities on the upstream and downstream side of vegetation patch respectively and V_c= critical velocity against critical depth.

3.2.2 Hydraulic jump classification in HDS

In case of hybrid defense system (HDS), in DVS and DVI cases, the hydraulic jump formed is classified as Type II and III as shown in Figure 6b and 6c. In these figures h_1, h_2 and h_3 are the average water depths infront of dyke, infront of vegetation and downstream of vegetation patch respectively, h_d = the average depth of water in the middle of L_{dv}, L_o = the length of start of hydraulic jump on the downstream slope of dyke from the toe of dyke towards the crest, L_{dv} = distance between dyke and vegetation, Fr_1 = Froude number on the upstream of dyke, Fr_o, h_o, V_o, V_1, V_2, V_c and L_j are already define previously. In Type II, hydraulic jump developed in section 2 with no jump in section 3. However, in Type III no jump formed in section 2 with only jump developed ~~on the downstream side of vegetation~~in section 3. The classification of hydraulic jump of HDS is described below and also summarized in Table 2.

In DVS model against the lower values of Froude number i.e; Fr_o = 0.40 and 0.44 weak jump (1.7<Fr<2.5 [47]) was formed in only section 2 (Type II) with small undulations in section 3 as shown in Figure 6b. For the initial values of Froude number (Fr_o = 0.40) the jump initiated on the bed in section 2, however, for Fr_o = 0.44 jump started from the downstream slope of the trapezoidal shape dyke. Air bubbles were also formed in section 2 and water surface slope also increases inside vegetation model. For Fr_o = 0.50 undular jump of Type II was formed in section 2. However, for higher values of Froude numbers i.e; Fr_o = 0.57, 0.60, 0.63 and 0.65 an undular hydraulic jump of Type III was formed as shown in Figure 6c.

Similarly, in DVI for Fr_o = 0.40 and 0.44 weak jump of Type II and for Fr_o = 0.50 and 0.57 undular jump of Type II was developed starting from the downstream slope of dyke (L_o increases with Froude number) as shown in Figure 6c. For Fr_o = 0.60, 0.60 and 0.65 undular jump of Type III was developed in section 3 with surface oscillations in section 2as shown in Figure 6c.

In DTMVS, DTMVI and DRMVI cases, the formation of hydraulic jumps were classified as Type IV, V and VI. The classification is based on the location of the formation of hydraulic jump either in section 2 (Type IV), in both section 2 and 3 (Type V) or in section 3 (Type VI). In DTMVS model for the lower values of Froude number i.e; Fr_o = 0.40, 0.44 undular jump of Type IV was observed as shown in Figure 6d. Air bubbles were also formed in section 2 and water surface slope also increases inside vegetation model. There was no jump for Fr_o = 0.50, 0.57 and 0.60, because hydraulic jump shifted its position from section 2 to section 3 from lower to higher Froude numbers. In this range the hydraulic jump was in transition state. For the remaining values of Fr_o = 0.63 and 0.65 undular hydraulic jump of Type VI was developed as shown in Figure 6e. The graphical representation of experimental results of DTMVS against all the values of the selected range of initial Froude number (Fr_o) are shown in Figure 8a.

In DTMVI model for Fr_o = 0.40, 0.44 and 0.50 jump of Type IV was observed (Figure 6d). The jump against Fr_o = 0.40 was weak and for Fr_o = 0.44 and 0.50 was undular in nature. For Fr_o = 0.57 undular jump was observed in both section 2 and section 3 classified as Type V as shown in Figure 6e and for Fr_o = 0.60, 0.63 and 0.65 undular jump developed was classified as Type VI. The graphical representation of experimental results of DTMVI against all the values of the selected range of initial Froude number (Fr_o) are shown in Figure 8b.

Similarly, in DRMVI model rectangular moat was used in combination with dyke and intermediate vegetation to examine the effect of the shape of moat on total energy dissipation. The profiles were same as in case of DTMVI. However, larger oscillations in between dyke and vegetation than DTMVI was observed due to rectangular shape, because in rectangular shape a sudden drop of water was observed due to the straight walls of moat while in trapezoidal moat due to sloping surface less oscillations were formed. Against the value of Fr_o = 0.40 weak jump of Type IV, for Fr_o = 0.44 and 0.50 undular jump of Type IV, for Fr_o = 0.57 undular jump of Type V was observed. For the remaining values of Fr_o = 0.60, 0.63 and 0.65 undular jump Type VI was developed as shown in Figure 6f..The graphical representation of experimental results of DRMVI against all the values of the selected range of initial Froude number (Fro) are shown in Figure 8c. The variation of length of hydraulic jump can be represented by relative length of hydraulic jump (Lj/y1) [40]. In these cases, the relative length of hydraulic jump (Lj/y1) increased *by increasing Frₒ and maximum relative jump was noted in case of DTMVI as compared to DTMVS and DRMVS as shown in Figure. 9.*Table 2: Hydraulic Jump classification of SDS and HDS

	Classification of Hydraulic jump						
	Froude Numbers						
Case ID	**0.40**	**0.44**	**0.50**	**0.57**	**0.60**	**0.63**	**0.65**
OVS	NJ	NJ	NJ	NJ	NJ	UJ, Type I	UJ, Type I
OVI	NJ	NJ	NJ	NJ	UJ, Type I	UJ, Type I	UJ, Type I
DVS	WJ, Type II	WJ, Type II	UJ, Type II	UJ, Type III	UJ, Type III	UJ, Type III	UJ, Type III
DVI	WJ, Type II	WJ, Type II	UJ, Type II	UJ, Type II	UJ, Type III	UJ, Type III	UJ, Type III
DTMVS	UJ, Type IV	UJ, Type IV	NJ	NJ	NJ	UJ, Type VI	UJ, Type VI
DTMVI	WJ, Type IV	UJ, Type IV	UJ, Type IV	UJ, Type V	UJ, Type VI	UJ, Type VI	UJ, Type VI
DRMVI	WJ, Type IV	UJ, Type IV	UJ, Type IV	UJ, Type V	UJ, Type VI	UJ, Type VI	UJ, Type VI

* Where, NJ = no jump, UJ = undular jump and WJ = week jump

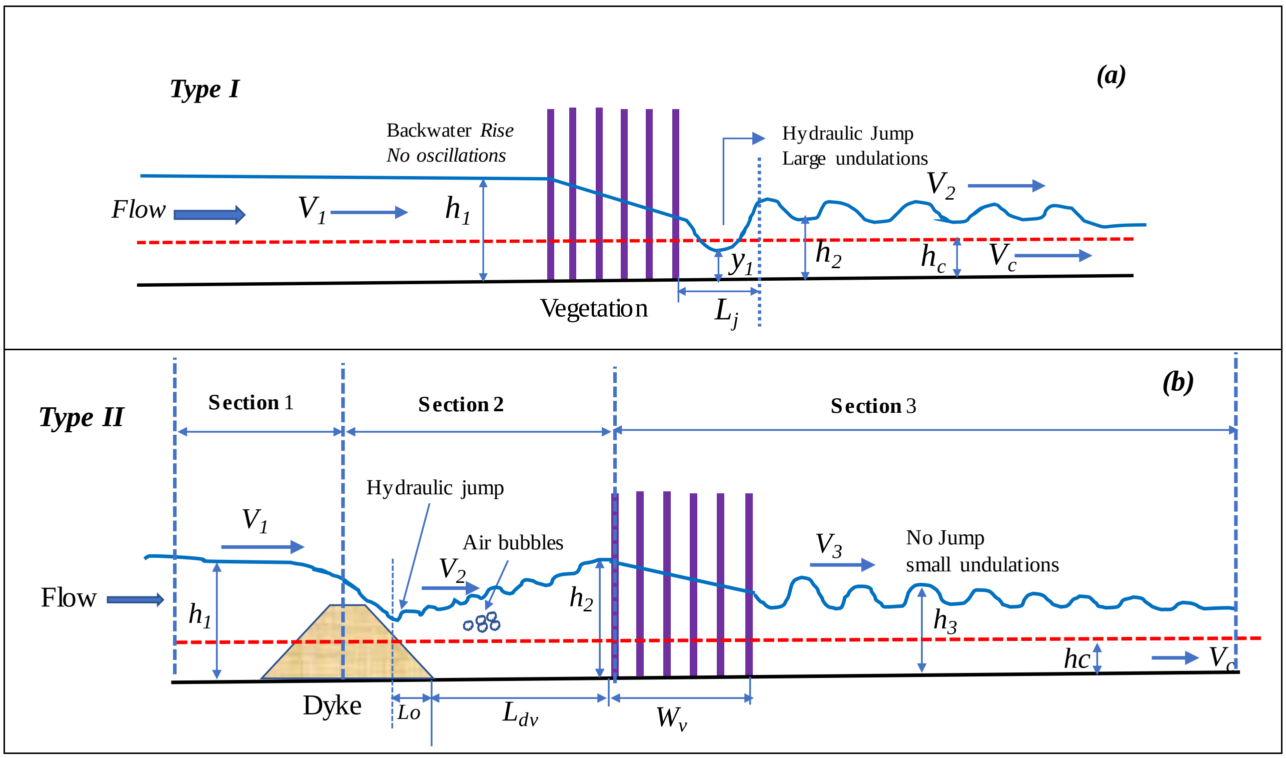

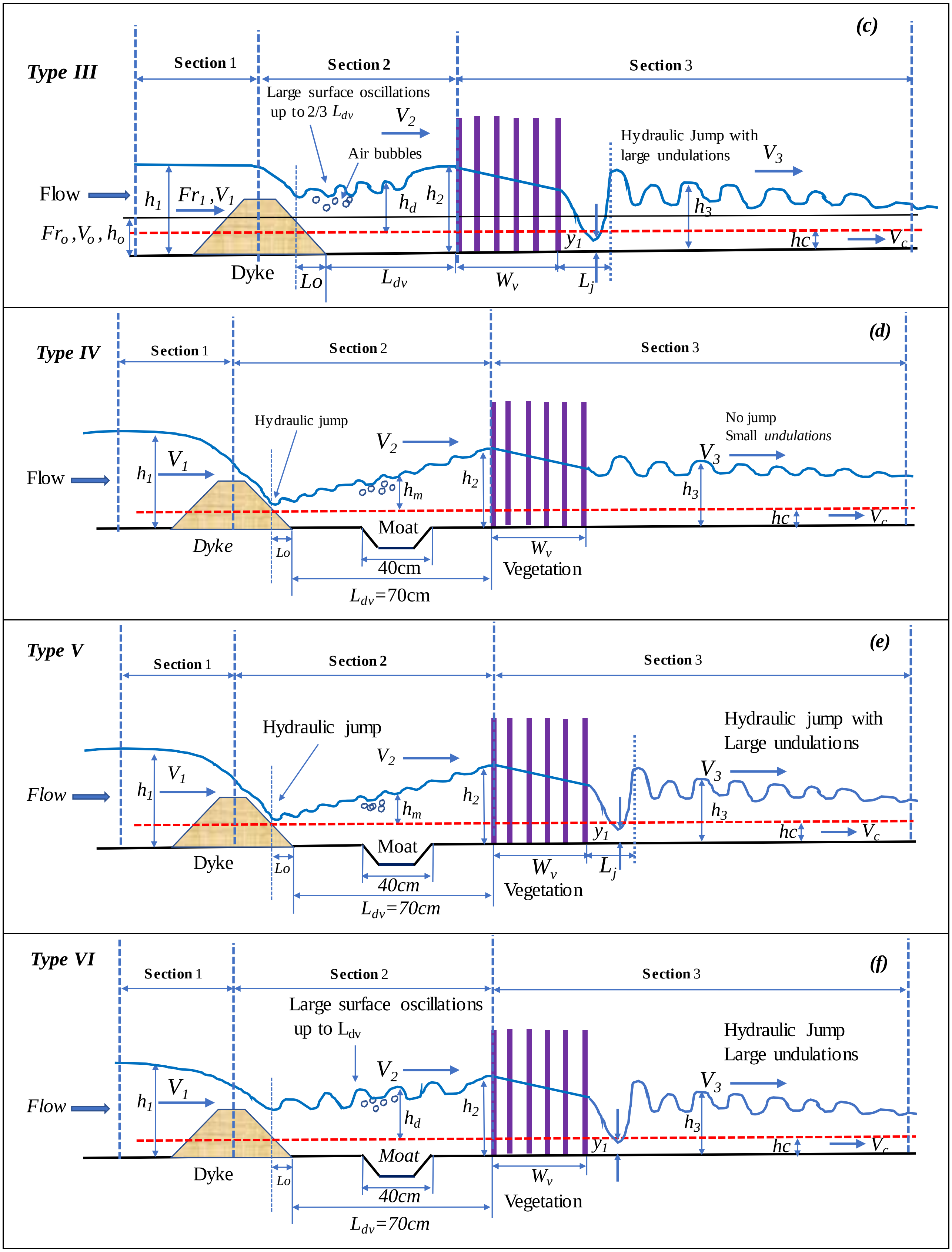
(c)
Type III
Section 1
Section 2
Section 3
Large surface oscillations up to 2/3 Ldv
V2
Air bubbles
Hydraulic Jump with large undulations
V3
Flow
h1
Fr1, V1
hd
h2
h3
Fro, Vo, ho
y1
hc
Vc
Dyke
Lo
Ldv
Wv
Lj
(d)
Type IV
Section 1
Section 2
Section 3
Hydraulic jump
V2
No jump
Small undulations
V3
V1
Flow
h1
hm
h2
h3
hc
Vc
Moat
Dyke
Lo
40cm
Wv
Vegetation
Ldv=70cm
(e)
Type V
Section 1
Section 2
Section 3
Hydraulic jump
V2
Hydraulic jump with
Large undulations
V3
V1
Flow
h1
hm
h2
h3
y1
hc
Vc
Moat
Dyke
Lo
40cm
Wv
Lj
Vegetation
Ldv=70cm
(f)
Type VI
Section 1
Section 2
Section 3
Large surface oscillations
up to Ldv
V2
Hydraulic Jump
Large undulations
V3
V1
Flow
h1
hd
h2
h3
y1
hc
Vc
Moat
Dyke
Lo
40cm
Wv
Vegetation
Ldv=70cm

Figure 6. Hydraulic jump and water surface classifications: [**OV model** (a) Jump on the downstream of vegetation (Type I)], [**DV model**: (b) Jump in section 2 only (Type II) (c) Jump in section 3 only (Type III)], [**DVM model**: (d) Jump in section 2 only (Type IV) (e) Jump in both section 2 and 3 (Type V)] (f) Jump in section 3 only (Type VI)

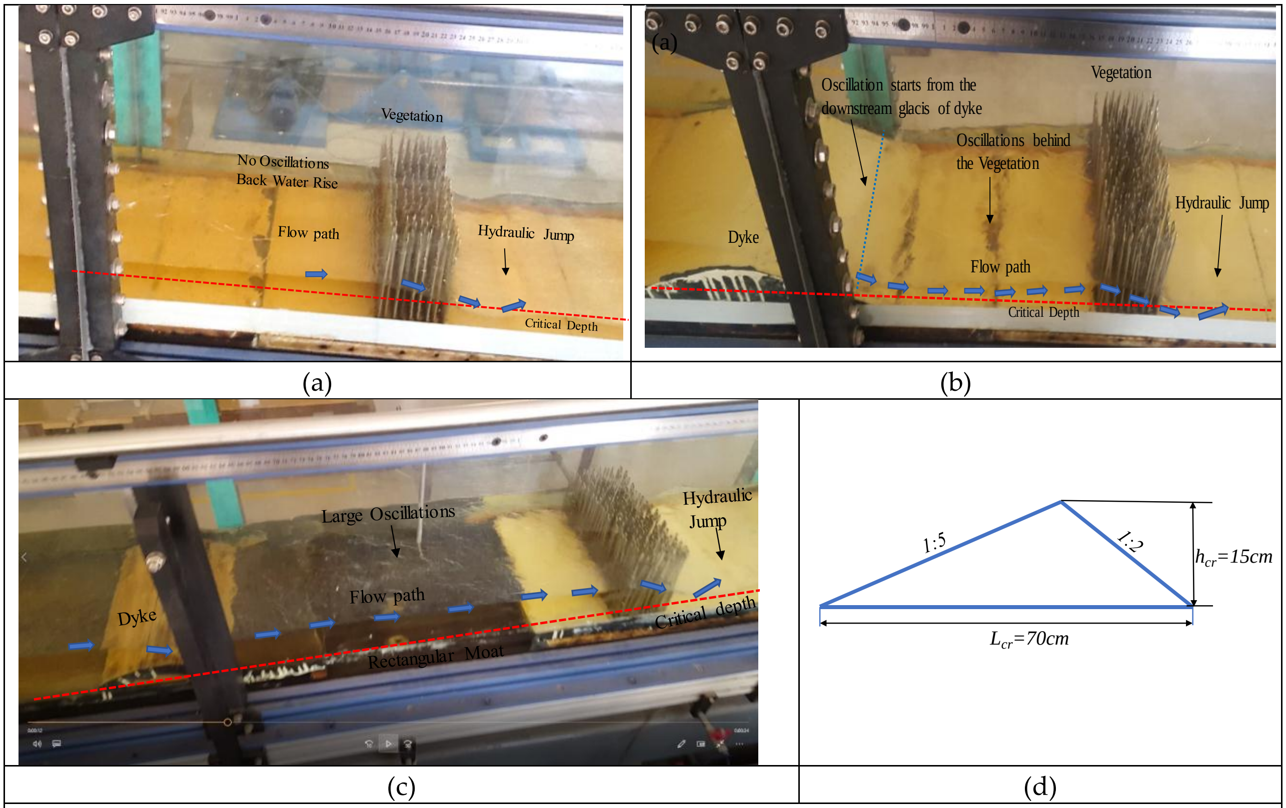

Figure 7. Experimental photographs: (a) OV model (b) DV model and (c) DMV model, (d) Crump weir model for delay time analysis

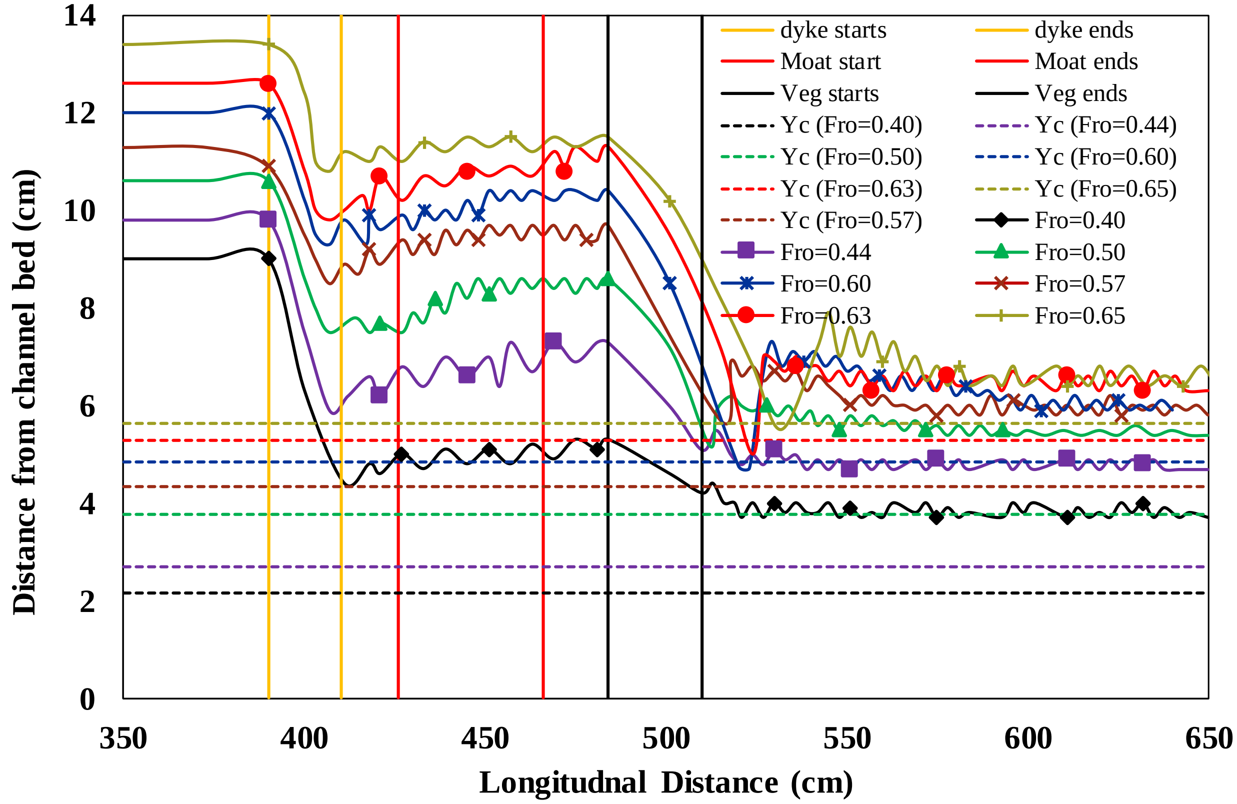

Distance from channel bed (cm)
Longitudnal Distance (cm)
0
2
4
6
8
10
12
14
350
400
450
500
550
600
650
dyke starts
dyke ends
Moat start
Moat ends
Veg starts
Veg ends
Yc (Fro=0.40)
Yc (Fro=0.44)
Yc (Fro=0.50)
Yc (Fro=0.60)
Yc (Fro=0.63)
Yc (Fro=0.65)
Yc (Fro=0.57)
Fro=0.40
Fro=0.44
Fro=0.50
Fro=0.60
Fro=0.57
Fro=0.63
Fro=0.65

(a)

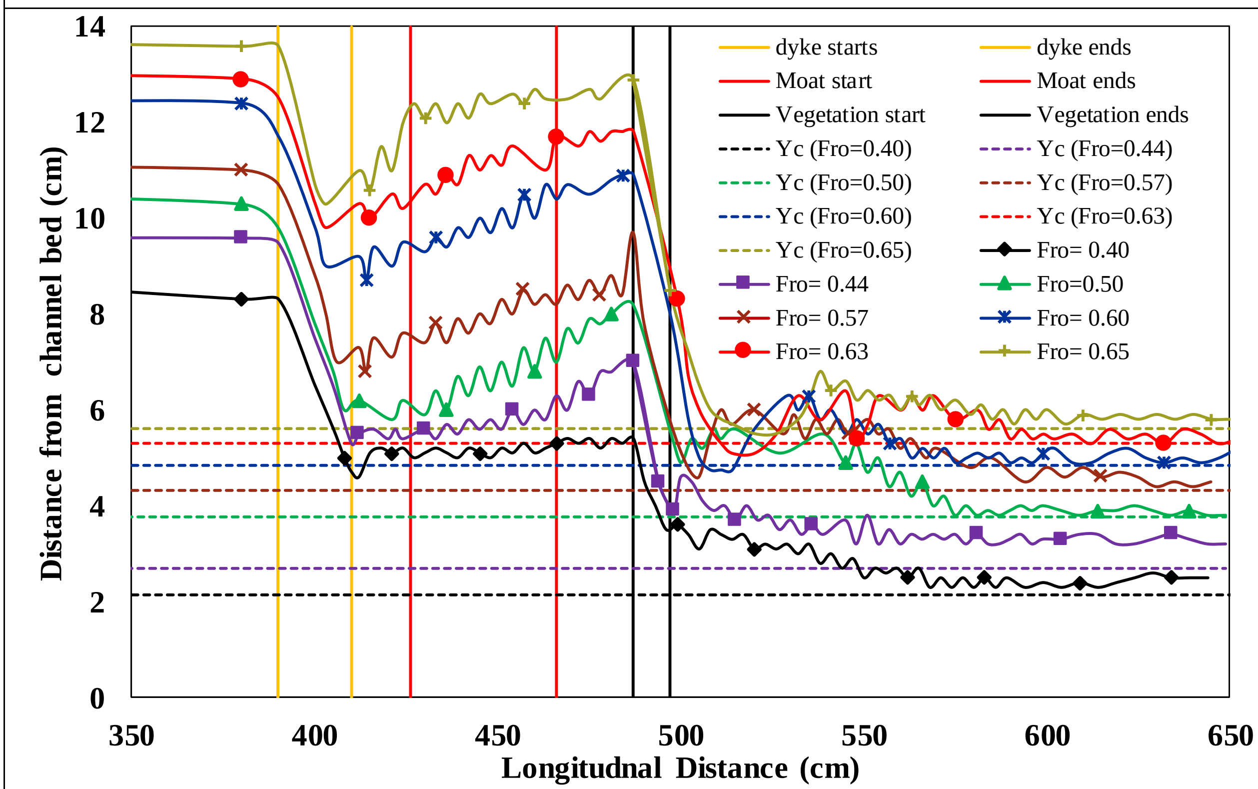

Distance from channel bed (cm)
Longitudnal Distance (cm)
0
2
4
6
8
10
12
14
350
400
450
500
550
600
650
dyke starts
dyke ends
Moat start
Moat ends
Vegetation start
Vegetation ends
Yc (Fro=0.40)
Yc (Fro=0.44)
Yc (Fro=0.50)
Yc (Fro=0.57)
Yc (Fro=0.60)
Yc (Fro=0.63)
Yc (Fro=0.65)
Fro= 0.40
Fro= 0.44
Fro=0.50
Fro= 0.57
Fro= 0.60
Fro= 0.63
Fro= 0.65

(b)

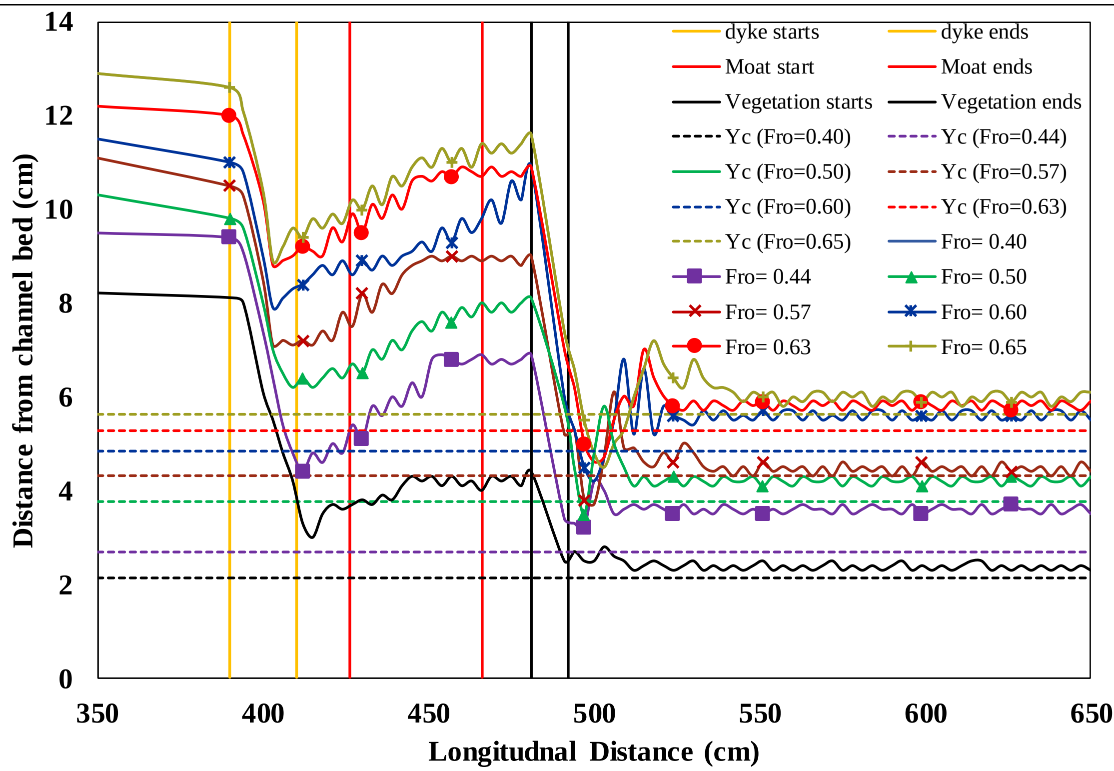

(c)

Figure 8. Experimental observations of water surface profiles (a) DTMVS, (b) DTMVI and (c) DRMVI

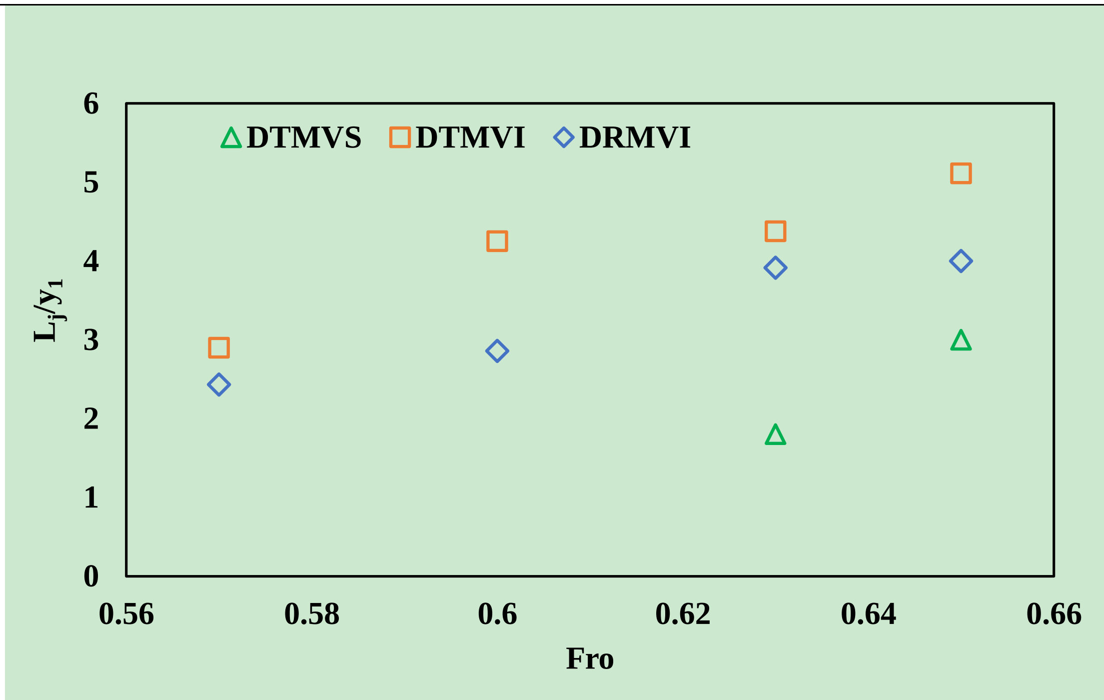

Figure. 9 Relative length of Hydraulic jump in HDS

3.3 Evaluation of Energy dissipation

3.3.1 Energy dissipation in single defense system (SDS)

Energy loss due to hydraulic jump and total energy loss wereas calculated against the Froude number range (Fr_o = 0.40-0.65). In this study, total energy loss for all the cases of SDS and HDS wais determined, however, energy loss due to hydraulic jump is explained only for HDS. ~~The energy loss in singly defense system is comprised of OVS and OVI.~~ For SDS, ~~T~~the maximum energy reduction in OVS and OVI was 28% and 36.34% respectively against Fr_o=0.40 and it decreased with higher values of Fr_o as shown in ~~(~~Figure 10a~~)~~. While increasing the values of Fr_o from 0.40 to 0.65 the energy dissipation rate decreased about 14.25% and 33.86% in OVS and OVI respectively. The average energy loss was 25.32% and 31.49% for OVS and OVI respectively. The results of energy dissipation show that initial Froude number and the density of vegetation (*B*/*D*) were the factors affecting the total energy loss. Based on these two important factors regression equations were developed for all the cases of SDS and HDS. In statistical analysis it is common to use 95% confidence interval [48].Various researchers used 95% confidence interval to better understand the spread of the estimated parameters [49] and also used in uncertainty analysis of different variables/parameters [50]. In this paper 95% confidence interval was used for two different variables to develop regression equations. Eq. 4 was developed to calculate the relative percentage energy loss in OVS and OVI.~~,~~

$$\frac{\Delta E_2}{E_2}(\%)=23.75[Fr_o]^{-0.47}\left[\frac{B}{D}\right]^{-0.31} \quad \ldots\ldots\ldots\ldots\ldots\ldots\ldots\ldots\ldots\ldots(4)$$

By using Eq. 4 the energy loss (%) of OVI and OVS calculated and compared with the experimental results (Eq. 3) as shown in Figure 11a. In this case the R^2 was 0.834 means that the experimental and computed values have close to each other.

3.3.2 Energy dissipation in hybrid defense system (HDS)

In HDS, the maximum energy loss (%) for DVS and DVI was 49.71% and 57.28% against Fr_o=0.40. While increasing the values of Fr_o from 0.40 to 0.65 the energy reduction rate decreased about 44% and 37.13% and the average energy loss was 36.63% and 41% respectively as shown in Figure 10b. The Eq. 5 was developed by regression analysis to compute the relative percentage energy reduction within the selected range of *Fro*. In this case the R^2 value was 0.95 in comparison between experimental (Eq. 2) and computed values (Eq. 5) (Figure 11b).

$$\frac{\Delta E_1}{E_1}(\%)=21.23[Fr_o]^{-1.09}\left[\frac{B}{D}\right]^{-0.218} \quad \ldots\ldots\ldots\ldots\ldots\ldots\ldots(5)$$

To check the effectiveness of all the cases of HDS i.e; DTMVS, DTMVI and DRMVI models, the maximum energy reduction due to hydraulic jump in section 2 (ΔE_{j2}), in section 3 (ΔE_{j3}), maximum overall energy dissipation and average energy dissipation were calculated (summary is shown in Table 3) In all these cases DTMVI performed better than DTMVS and DRMVI. In case of DTMVI maximum ΔE_{j2} = 27% and ΔE_{j3} = 4%, the maximum total energy reduced in this case was 60% and the average energy reduced was 46%.

The Figure 10(c) shows the combine trends of DTMVS, DTMVI and DRMVI. To compare the results of average energy loss in SDS and HDS, standard error bars are presented in ~~The average energy reduction in all the cases are elaborated in~~ Figure 11(d). In this figure the error bars of SDS are not overlapping with

HDS and by convention, the overlapping standard error bars have no significant difference [51]. It was resulted that there was a significant difference between the average values of energy dissipation between SDS and HDS exist. Based on the data of DTMVS, DTMVI and DRMVI cases, Eq. 6 was developed ~~by regression analysis with 95% confidence interval.~~to compute the relative percentage energy loss. The experimental (Eq. 2) and computed (Eq. 6) results showed acceptable relation as R^2 value was 0.91. The comparison is shown in Figure 11c.

$$\frac{\Delta E_1}{E_1}(\%)=22.14[Fr_o]^{-1.04}\left[\frac{B}{D}\right]^{-0.1584} \text{..............................(6)}$$

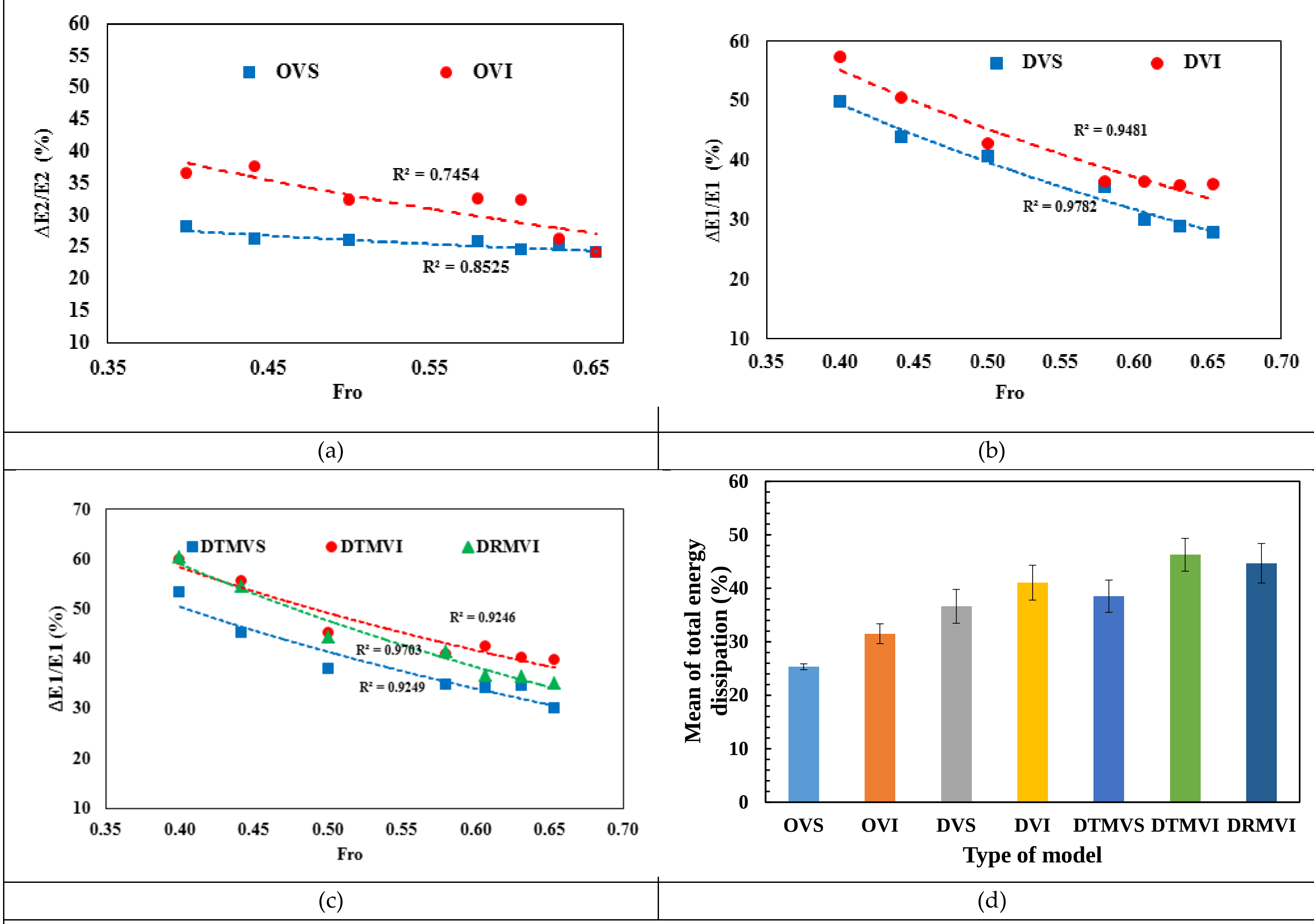

Figure 10. Percentage energy loss: (a) OV, (b) DV and (c) DMV (d) Average energy reduction comparison for all cases

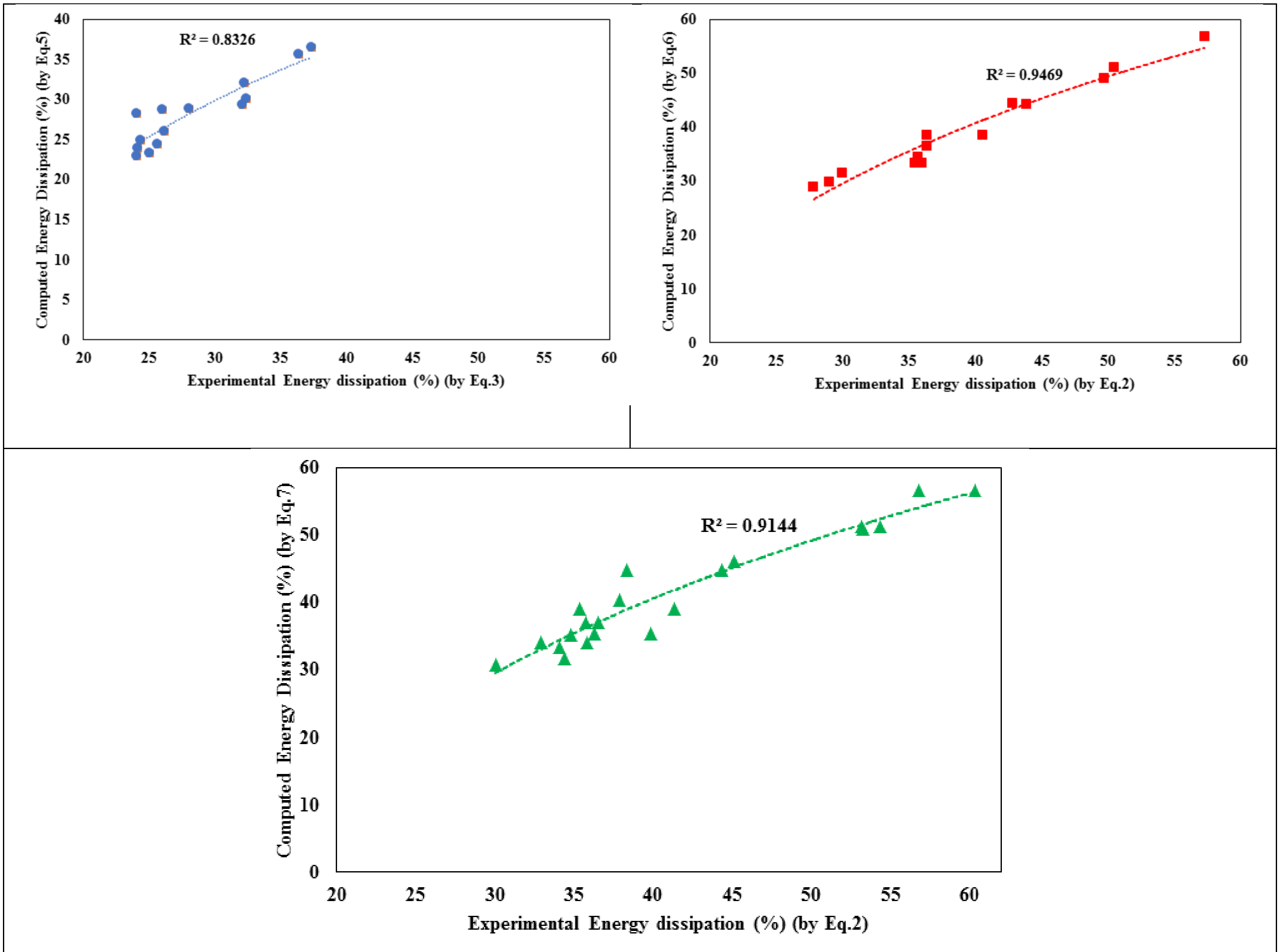

Figure 11. Experimental and computed results comparison: (a) OVS & OVI, (b) DVS & DVI and (c) DTMVS, DTMVI and DRMVI

Table 3. Summary of Energy dissipation of HDS.

Case ID	Energy loss due to hydraulic jump		Average Energy loss (%)	Maximum Energy loss (%)
	ΔE_{j2} (%)	ΔE_{j3} (%)		
DTMVS	24	2.84	38.52	53.26
DTMVI	27	4	46	60
DRMVI	22	3	43.75	60

3.4 Delay in flood water arrival time and water level rise

In the first step delay time T_{WM} was computed without placing model in the flume. Similarly, the delay time for single defense system and hybrid defense system were computed. Against the different values of initial Froude No., T_{WM} was in the range of 28s-80s, whereas it was 29-115s for OVS, 30-118s for OVI, 32-129s for DVS and 34-132s for DVI. Similarly delay time for DTMVS, DTMVI and DRMVI was 33-137s, 37s-140s and 36-139 respectively. The maximum delay time was 2 min 20 sec for DTMVI against Fr_o = 0.40. In all the cases the delay time decreases by increasing Fr_o. The relative time with respect to T_{WM} was also maximum in case of DTVMI, which will result in maximum delay in flood arrival.

To examine the relationship between two or more variables, the ANOVA test was performed by the researchers [41]. The same test was applied in this paper to examine the relative delay time of SDS and HDS and to incorporate the multiple comparisons of pairwise differences within each level of Froude numbers. In this test seven different groups were considered (Table 4). The sum of square (SS), degree of freedom (Df), mean square (MS), F values, P-value and the value of F critical were calculated. Let suppose Ho = null hypothesis i.e; the mean of all the cases were equal. By convention if $P < 0.05$ the result is statistically significant [51]. The P-value was found less than 0.05 in this test. It is also found that F > F-critical, so null hypothesis was rejected [52]. That means that at least one value of mean of a data set is significantly different than the other data sets. The summary is shown in Table 4 below.

Table 4:ANOVA test summary

SUMMARY

Groups	Count	Sum	Average	Variance
TOVI/TWM	7	8.15	1.165	0.027
TOVS/TWM	7	7.8	1.11	0.028
TDVI/TWM	7	8.72	1.24	0.052
TDVS/TWM	7	8.23	1.17	0.058
TDTMVS /TWM	7	9.22	1.31	0.043
TDTMVI / TWM	7	9.83	1.4	0.031
TDRVMI / TWM	7	9.77	1.39	0.031

ANOVA

Source of Variation	SS	Df	MS	F	P-value	F crit
Between Groups	0.56	6	0.0934	2.4	0.043	2.32
Within Groups	1.632	42	0.0388			
Total	2.192	48				

The standard error bars were represented against the relative time of delay for each case of SDS and HDS (Figure 12). The results show that there is no significant difference between the means of OVS, OVI, DVS and DVI because the error bars are overlapping. However, the standard error bars of DTMVS, DTMVI and DRMVI are not overlapping with OVS, OVI, DVS and DVI resulting that there is a significant difference exist in means values of these models. So, it is concluded that the delay time of HDS is higher than SDS.

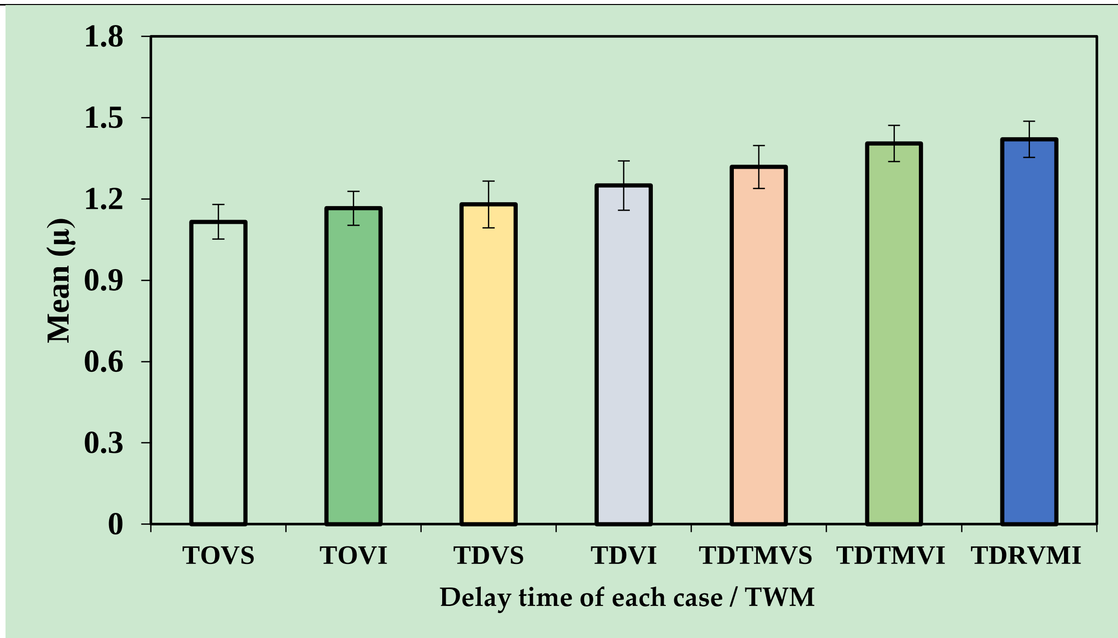

Figure 12. Comparison of relative delay time of SDS and HDS with standard error bars

4. *Discussion*

In this paper single and hybrid defense systems were tested in relation to the backwater rise, relative energy dissipation and relative delay time of flood. In SDS vegetation of variable densities (*B*/*d*) were considered without any other model as many researchers did in the past [40,44]. Vegetation of different densities i.e; dense (*B*/*d*=0.25), intermediate (*B*/*d*=1.09) and sparse vegetation (*B*/*d*=2.13) were used in the past [40]. However only intermediate and sparse vegetation were selected for this paper because the denser vegetation (*B*/*d*=0.25) is rare and difficult to construct in the field. Various researchers classified the hydraulic jump as breaking and non-breaking undular jump based on b/y1 [53] and h_o/L [40], where b = width of channel, y1 = depth of water at the toe of hydraulic jump, h_o = initial water depth and L = wave length. In this study for OVS and OVI undular hydraulic jump was observed only for the higher values of Fr_o (0.60, 0.63 and 0.65) and no jump was observed for lower values of Fr_o. The similar results were found in the literature [40]. The relative energy dissipation for a vegetation thickness of dn-180 No. cm calculated by Pasha and Tanaka (2017) was 26–28% and 29–32% in sparse and intermediate vegetation respectively. However, in the current research the relative energy dissipated was in the range of 24-28% and 24-36% in sparse and intermediate vegetation respectively. The range of Fr_o used by Pasha and Tanaka (2017) was 0.57 to 0.73 and in this study it was 0.40 to 0.65. The back water rise increases by increasing the density of vegetation [44]. The back water rise was observed higher in OVI than OVS as shown in Figure 5a.

Previously, the coastal structures, trees and houses were damaged when Great East Tsunami in Japan overtopped the existing embankment [54]. Thus, a secondary structure on the downstream side of the embankment is required to reduce the flow velocity. The hydraulic jump is formed after placing any structure on the downstream of embankment [45]. In this regard a secondary structure of different layers of single and double layer vegetation on the downstream of embankment was tested recently [55]. The selected range of Fr_o was 1.08-1.56. The hydraulic jump was classified on the basis of the location of its generation. The jump classified was jump A (formed on the bed of channel) and jump B (formed on the downstream slope of embankment). According to that study for the initial values of Fr_o, Type A jump was formed on the bed of the channel in between embankment and vegetation while Type B jump was observed for the higher values of Fr_o. In few cases the jump started inside the vegetation patch and the range of Froude number of hydraulic jump was 2<Fr<4.49. The maximum energy dissipated due to jump was 39% and the maximum total energy reduction was in between 27% and 54% [55]. The hydraulic jump based on the values of Froude number was also classified by 2-D numerical analysis in the previous study [56].

In the present study for DVS and DVI, the hydraulic jump was classified against the lower values Fr_o (0.40-0.57) was observed. However for higher values i.e; Fr_o (0.60, 0.63 and 0.65) the jump formed was only on the downstream of vegetation and no jump was observed in between dyke and vegetation. This is due to the reason that the height of dyke and the distance between the downstream toe of dyke to the start of vegetation was 14.5 cm and 50 cm respectively in the previous study [55], however, in the present case the height of dyke was 5.5 cm and distance between dyke and vegetation was 70 cm. As the density of vegetation increases the energy reduction rate also increases [57].The total relative energy reduction for DVS and DVI was in between 28% and 57% and the average relative energy dissipation was 37% and 41% in DVS and DVI respectively.

In case of extreme flood events or Tsunamis, hybrid defense system of the combination of artificial and natural structures are recommended to reduce the devastating effects [58]. These hybrid defense systems are used to enhance coastal resilience in the protection from coastal flooding [59]. Recently, hybrid defense system comprising of dyke, moat and vegetation was tested by changing the layout of the components. The fluid force, tsunami arrival time and overflow volume for different cases were measured. The hybrid defense system in the order of vegetation, a trapezoidal moat, and an embankment performed best in relation to the overflow volume, arrival time and fluid force[32].

In the current paper a hybrid system in the order of dyke, moat (trapezoidal and rectangular) and vegetation of variable densities were tested. Backwater rise, energy dissipation due to hydraulic jump and total relative energy dissipation were measured for each case to clarify the optimal hybrid defense system. To examine the effect of shape of the moat, rectangular and trapezoidal shapes were used. For DTMVS, DTMVI and DRMVI weak and undular jumps of Type IV, V and VI were observed. The maximum back water rise was observed for DTMVI case due to the fact that the denser vegetation offered more resistance to flow resulting in higher back water rise as shown in Figure 5a. The energy loss due to hydraulic jump was usually low [45] and the fraction of energy dissipated due to undular jump is less than 5% [60]. In the current study, the amount of energy dissipation due undular jump on the downstream side of vegetation was well below 5% (ΔE_{j3} in Table 3). The maximum total relative energy dissipation and maximum average energy dissipation by hybrid defense system was 60% and 46% in DTMVI model. The arrival time was also highest in DTMVI case. Contrarily, the hybrid defense system in the order of vegetation, moat and dyke (where vegetation is on seaward side) performed best in the previous study [32]. However in this combination in case of a devastating flood event the water may overtop the embankment and it will be difficult to join this water to the river. Secondly, there was no space considered in between the moat and embankment by Zaha (2019) [32] and in case of the breaching or erosion of embankment the moat may fill with the erodible material that will not serve as a moat after filling.

In the current research the combination of dyke, moat and vegetation (where dyke was on the river side) was tested and in case of overtopping flow the water will come back to the moat and it will further join the river by seepage action or water will store in the moat to act as a flood harvesting structure. Moreover, the space between the downstream toe of dyke and the start of moat (L_{dv}) was kept 15 cm to ensure the safety of the moat structure in case of breaching of dyke. The rectangular moat was less effective than the trapezoidal moat based on the total energy loss and the arrival time. The sides of a rectangular hydraulic structure are also not stable. In the light of the results obtained a hybrid defense system in the order of dyke, trapezoidal moat and intermediate vegetation is highly recommended. The limitation of the proposed system is the space available to construct the defense system. In case of non-availability of the space single defense system will be preferred. More shapes and different dimensions of moat should be tested for energy dissipation and the role of moat with respect to flood water harvesting should also be investigated in future.

5. Conclusions

The flow structure with energy loss in a subcritical flow against the selected range of initial Froude numbers (Fr_o = 0.40–0.65) around Single Defense System (SDS) and the Hybrid Defense System (HDS) were investigated experimentally in a water flume. The main conclusions of the study are as follows

- The backwater rise was maximum for OVI and DTMVI in SDS and HDS respectively. The backwater rise is directly proportional to the density of vegetation (B/d) and initial Froude number (Fr_o). The water surface slope also increased by increasing vegetation density. The denser and wider the vegetation, the larger is the total energy dissipation in both SDS and HDS cases.
- In SDS only undular hydraulic jumps can be observed in both OVS and OVI, resulting in a significant energy loss. In HDS weak and undular hydraulic jumps were observed and the maximum energy loss due to hydraulic jump ΔE_{j2} =27% and ΔE_{j3}= 4% in DTMVI case. The maximum total energy reduced in this case was 60% and the average energy reduced was 46%. Similarly, in case of DRMVI the maximum value of energy loss due to hydraulic jump ΔE_{j2} =22% and ΔE_{j3}= 3% respectively. The maximum total energy reduction and average energy reduction were 60% and 43.75% respectively. In all these cases the rate of energy reduction due to the hydraulic jump decreases by increasing Fr_o.
- The performance of the DTMVI model to delay the arrival time of flood water is the highest among all the models investigated in this paper.

- The "moat" can serve as flood water harvesting and increasing the response time of flash floods generated from hill torrents. The shape of the moat affects the reduction of energy in general; however, its trapezoidal shape performs better than rectangular shape.

Under the above conclusions, a hybrid defense system is highly recommended where the enough space is available across the river flow. The proposed system will be highly effective in various flood plains similar to that of Indus River.

Authors Contributions: Conceptualization, Afzal Ahmed and Abdul Razzaq Ghumman; Data curation, Afzal Ahmed; Investigation, Afzal Ahmed; Methodology, Afzal Ahmed; Supervision, Abdul Razzaq Ghumman; Writing – original draft, Afzal Ahmed; Writing – review & editing, Abdul Razzaq Ghumman.

Acknowledgements:

This study was funded by University of Engineering & Technology, Taxila, Pakistan. The authors acknowledge Dr. Ghufran Ahmed Pasha for his useful comments and great help during whole of this research.

Conflict of interest: The authors declare no conflict of interest

References:

[1] Smith,K., *Environmental hazards: assessing risk and reducing disaster*, **2003**,. Routledge.

[2] Kellens,W.;Terpstra,T.;De Maeyer,P., Perception and Communication of Flood Risks: A Systematic Review of Empirical Research, *Risk Anal.*, **2013**, *33*, 24–49.

[3] Buijs,J.;Boelens,L.;Bormann,H.;Restemeyer,B.;Terpstra,T.;van der Voorn,T., Adaptive planning for flood resilient areas: dealing with complexity in decision-making about multilayered flood risk management. AESOP conference paper, in *16th meeting: Adaptive Planning for Spatial Transformation, Groningen, Netherlands*, **2018**,.

[4] Ali Hasan Muhammad;Tanaka, Energy Reduction of a Tsunami Current through a Hybrid Defense System Comprising a Sea Embankment Followed by a Coastal Forest, *Geosciences*, **2019**, *9*, 247.

[5] Suppasri,A.;Shuto,N.;Imamura,F.;Koshimura,S.;Mas,E.;Yalciner,A. C., Lessons learned from the 2011 Great East Japan tsunami: Performance of tsunami countermeasures, coastal buildings, and tsunami evacuation in Japan, *Pure Appl. Geophys.*, **2013**, *170*, 993–1018.

[6] Nandasena,N. A. K.;Sasaki,Y.;Tanaka,N., Modeling field observations of the 2011 Great East Japan tsunami: Efficacy of artificial and natural structures on tsunami mitigation, *Coast. Eng.*, **2012**, *67*, 1–13.

[7] Pakoksung,K.;Suppasri,A.;Imamura,F., Systematic Evaluation of Different Infrastructure Systems for Tsunami Defense in Sendai City, *Geosciences*, **2018**, *8*, 173.

[8] Abbas,A.;Amjath-Babu,T. S.;Kächele,H.;Müller,K., Non-structural flood risk mitigation under developing country conditions: an analysis on the determinants of willingness to pay for flood

insurance in rural Pakistan, *Nat. Hazards*, **2015**, *75*, 2119–2135.

[9] Houze Jr,R. A.;McMurdie,L. A.;Rasmussen,K. L.;Kumar,A.;Chaplin,M. M., Multiscale aspects of the storm producing the June 2013 flooding in Uttarakhand, India, *Mon. Weather Rev.*, **2017**, *145*, 4447–4466.

[10] van Oldenborgh,G. J.;Otto,F. E. L.;Haustein,K.;AchutaRao,K., The heavy precipitation event of December 2015 in Chennai, India, *Bull. Am. Meteorol. Soc.*, **2016**, *97*, S87–S91.

[11] Philip,S. *et al.*, Attributing the 2017 Bangladesh floods from meteorological and hydrological perspectives, *Hydrol. Earth Syst. Sci.*, **2019**, *23*, 1409–1429.

[12] Marfai,M. A.;Hizbaron,D. R., Community's adaptive capacity due to coastal flooding in Semarang coastal city, Indonesia, *Int. J. Ser. Geogr. Ann. Univ. Oradea*, **2011**, *21*, 2011.

[13] Marfai,M. A.;King,L., Potential vulnerability implications of coastal inundation due to sea level rise for the coastal zone of Semarang city, Indonesia, *Environ. Geol.*, **2008**, *54*, 1235–1245.

[14] Zhao,G.;Visser,P. J., Flow Process of the Embankment Breaching, **2013**,.

[15] Evangelista,S., Experiments and numerical simulations of dike erosion due to a wave impact, *Water (Switzerland)*, **2015**, *7*, 5831–5848.

[16] Greco,M.;Iervolino,M.;Leopardi,A.;Vacca,A., A two-phase model for fast geomorphic shallow flows, *Int. J. Sediment Res.*, **2012**, *27*, 409–425.

[17] Dewals,B.;Rulot,F.;Erpicum,S.;Archambeau,P.;Pirotto,M., Advanced Topics in Sediment Transport Modelling: Non-alluvial Beds and Hyperconcentrated Flows, *Sediment Transp.*, **2012**,.

[18] Tanaka,N., Vegetation bioshields for tsunami mitigation: review of effectiveness, limitations, construction, and sustainable management, *Landsc. Ecol. Eng.*, **2009**, *5*, 71–79.

[19] Peruzzo,P.;de Serio,F.;Defina,A.;Mossa,M., Wave height attenuation and flow resistance due to emergent or near-emergent vegetation, *Water (Switzerland)*, **2018**, *10*, 1–13.

[20] Sanjou,M.;Okamoto,T.;Nezu,I., Experimental study on fluid energy reduction through a flood protection forest, *J. Flood Risk Manag.*, **2018**, *11*.

[21] Anjum,N.;Ghani,U.;Pasha,G. A.;Latif,A.;Sultan,T.;Ali,S., To investigate the flow structure of discontinuous vegetation patches of two vertically different layers in an open channel, *Water (Switzerland)*, **2018**, *10*.

[22] Mulahasan,S.;Stoesser,T., Flow resistance of in-line vegetation in open channel flow, *Int. J. River Basin Manag.*, **2017**, *15*, 329–334.

[23] Thuy,N. B., Flow and potential force due to runup tsunami around a coastal forest with a gap – experiments and numerical simulations, *Int. J. Tsunami Soc.*, **2010**, *20*, 57–102.

[24] Liu,J. *et al.*, Water conservancy projects in China: Achievements, challenges and way forward, *Glob. Environ. Chang.*, **2013**, *23*, 633–643.

[25] Dalimunthe,S. A., Who manages space? Eco-DRR and the local community, *Sustain.*, **2018**, *10*, 1–18.

[26] Västilä,K.;Järvelä,J.;Aberle,J., Characteristic reference areas for estimating flow resistance of natural foliated vegetation, *J. Hydrol.*, **2013**, *492*, 49–60.

[27] Mcdonald,T.;Gann,G. D.;Jonson,J.;Dixon,K. W., International standards for the practice of ecological restoration- including principles and key concepts, *Society for ecological restoration*, **2016**, 1.

[28] Pasha,G. A.;Tanaka,N.;Yagisawa,J.;Achmad,F. N., Tsunami mitigation by combination of coastal vegetation and a backward-facing step, *Coast. Eng. J.*, **2018**, *60*, 1–22.

[29] Tanaka,N.;Yasuda,S.;Iimura,K.;Yagisawa,J., Combined effects of coastal forest and sea embankment on reducing the washout region of houses in the Great East Japan tsunami, *J. Hydro-Environment Res.*, **2014**, *8*, 270–280.

[30] Fadly,U.;Murakami,K., Study on Reducing Tsunami Inundation Energy By the Modification of Topography Based on Local Wisdom, *J. Japan Soc. Civ. Eng. Ser. B3 (Ocean Eng.*, **2013**, *68*, I_66-I_71.

[31] Tanaka,N.;Igarashi,Y., Multiple defense for tsunami inundation by two embankment system and prevention of oscillation by trees on embankment, in *Proceedings of 20th Congress of IAHR APD Congress*, **2016**, 1–8.

[32] Zaha,T.;Tanaka,N.;Kimiwada,Y., Flume experiments on optimal arrangement of hybrid defense system comprising an embankment, moat, and emergent vegetation to mitigate inundating tsunami current, *Ocean Eng.*, **2019**, *173*, 45–57.

[33] Tariq,M. A. U. R.;Van de Giesen,N., Floods and flood management in Pakistan, *Phys. Chem. Earth*, **2012**, *47–48*, 11–20.

[34] Aslam,M., Flood Management Current State, Challenges and Prospects in Pakistan: A Review, *Mehran Univ. Res. J. Eng. Technol.*, **2018**, *37*, 297–314.

[35] Tanvir,M. A.;Siddiqui,M. T.;Shah,A. H., Growth and price trend of Eucalyptus camaldulensis in Central Punjab, *Int. J. Agric. Biol.*, **2002**, *4*, 344–346.

[36] Huai,W. X.;Zeng,Y. H.;Xu,Z. G.;Yang,Z. H., Three-layer model for vertical velocity distribution in open channel flow with submerged rigid vegetation, *Adv. Water Resour.*, **2009**, *32*, 487–492.

[37] Huai,W.;Wang,W.;Hu,Y.;Zeng,Y.;Yang,Z., Analytical model of the mean velocity distribution in an open channel with double-layered rigid vegetation, *Adv. Water Resour.*, **2014**, *69*, 106–113.

[38] Pasha,G. A.;Tanaka,N., Critical Resistance Affecting Sub- to Super-Critical Transition Flow by Vegetation, *J. Earthq. Tsunami*, **2019**, *13*, 1950004.

[39] Lakusic,S., Reference water levels for the design of dykes and earthfill dams, *J. Croat. Assoc. Civ. Eng.*, **2018**, *70*, 225–233.

[40] Pasha,G. A.;Tanaka,N., Undular hydraulic jump formation and energy loss in a flow through emergent vegetation of varying thickness and density, *Ocean Eng.*, **2017**, *141*, 308–325.

[41] Pietro,D.;Alpaos,A. D.;Carniello,L.;Defina,A., Advances in Water Resources Mathematical modeling of flooding due to river bank failure, *Adv. Water Resour.*, **2013**, *59*, 82–94.

[42] Tanaka,N.;Yagisawa,J., Flow structures and sedimentation characteristics around clump-type vegetation, *J. Hydro-environment Res.*, **2010**, *4*, 15–25.

[43] Novak,P.;Guinot,V.;Jeffrey,A.;Reeve,D. E., *Hydraulic modelling: An introduction: Principles, methods and applications*, **2018**,. CRC Press.

[44] Iimura,K.;Tanaka,N., Numerical simulation estimating effects of tree density distribution in coastal forest on tsunami mitigation, *Ocean Eng.*, **2012**, *54*, 223–232.

[45] Chow,V. T., Open-channel hydraulics, in *Open-channel hydraulics*, **1959**, McGraw-Hill.

[46] Hager,W. H., B-jump in sloping channel, *J. Hydraul. Res.*, **1988**, *26*, 539–558.

[47] Jesudhas,V.;Murzyn,F.;Balachandar,R., IDDES Evaluation of Oscillating Hydraulic Jumps, *E3S Web Conf.*, **2018**, *40*, 05067.

[48] Brown,A. M., A step-by-step guide to non-linear regression analysis of experimental data using a Microsoft Excel spreadsheet, **2001**, *65*, 191–200.

[49] Water Resources Research, **2016**, 1899–1922.

[50] Cheng,N.;Nguyen,H. T., Hydraulic Radius for Evaluating Resistance Induced by Simulated Emergent Vegetation in Open-Channel Flows, **2011**, 995–1004.

[51] Cumming,G.;Fidler,F.;Vaux,D. L., Error bars in experimental biology, **2007**, *177*, 7–11.

[52] Science,E., Investigation of flood pattern using ANOVA statistic and remote sensing in Malaysia Investigation of flood pattern using ANOVA statistic and remote sensing in Malaysia.

[53] Ohtsu,I.;Yasuda,Y.;Gotoh,H., Flow conditions of undular hydraulic jumps in horizontal rectangular channels, *J. Hydraul. Eng.*, **2003**, *129*, 948–955.

[54] Tanaka,N.;Sato,M., Scoured depth and length of pools and ditches generated by overtopping flow from embankments during the 2011 Great East Japan Tsunami, *Ocean Eng.*, **2015**, *109*, 72–82.

[55] Ali,R.;Muhammad,H.;Tanaka,N., Energy Reduction of a Tsunami Current through a Hybrid Defense System Comprising a Sea Embankment Followed by a Coastal Forest, **2019**, 1–27.

[56] Luo,C., Hydraulic jump- the state of the art hydrodynamic characteristics of fixed and moveable beds, *International Journal of Applied Engineering and Technology*, **2015**, *5(2)*

[57] Tanaka,N.;Sasaki,Y.;Mowjood,M. I. M.;Jinadasa,K.;Homchuen,S., Coastal vegetation structures and their functions in tsunami protection: experience of the recent Indian Ocean tsunami, *Landsc. Ecol. Eng.*, **2007**, *3*, 33–45.

[58] Temmerman,S.;Meire,P.;Bouma,T. J.;Herman,P. M. J.;Ysebaert,T.;De Vriend,H. J., Ecosystem-based coastal defence in the face of global change, *Nature*, **2013**, *504*, 79.

[59] Sutton-Grier,A. E.;Wowk,K.;Bamford,H., Future of our coasts: The potential for natural and hybrid infrastructure to enhance the resilience of our coastal communities, economies and ecosystems, *Environ. Sci. Policy*, **2015**, *51*, 137–148.

[60] Streeter,V. L.;Wylie,E. B., Fluid mechanics, 1979. McGraw-Hill, New York.